

947
948
949
950
951
952
953
954
955
956
957
958
959
960
961
962
963
964
965
966
967
968
969
970
971
972
973
974
975
976
977

Supplemental Information

Naive human B cells engage the receptor binding domain of SARS-CoV-2, variants of concern, and related sarbecoviruses

Jared Feldman^{1†}, Julia Bals^{1†}, Clara G. Altomare², Kerri St. Denis¹, Evan C. Lam¹, Blake M. Hauser¹, Larance Ronsard¹, Maya Sangesland¹, Thalia Bracamonte Moreno¹, Vintus Okonkwo¹, Nathania Hartojo¹, Alejandro B. Balazs¹, Goran Bajic², Daniel Lingwood^{1*} and Aaron G. Schmidt^{1,3*}

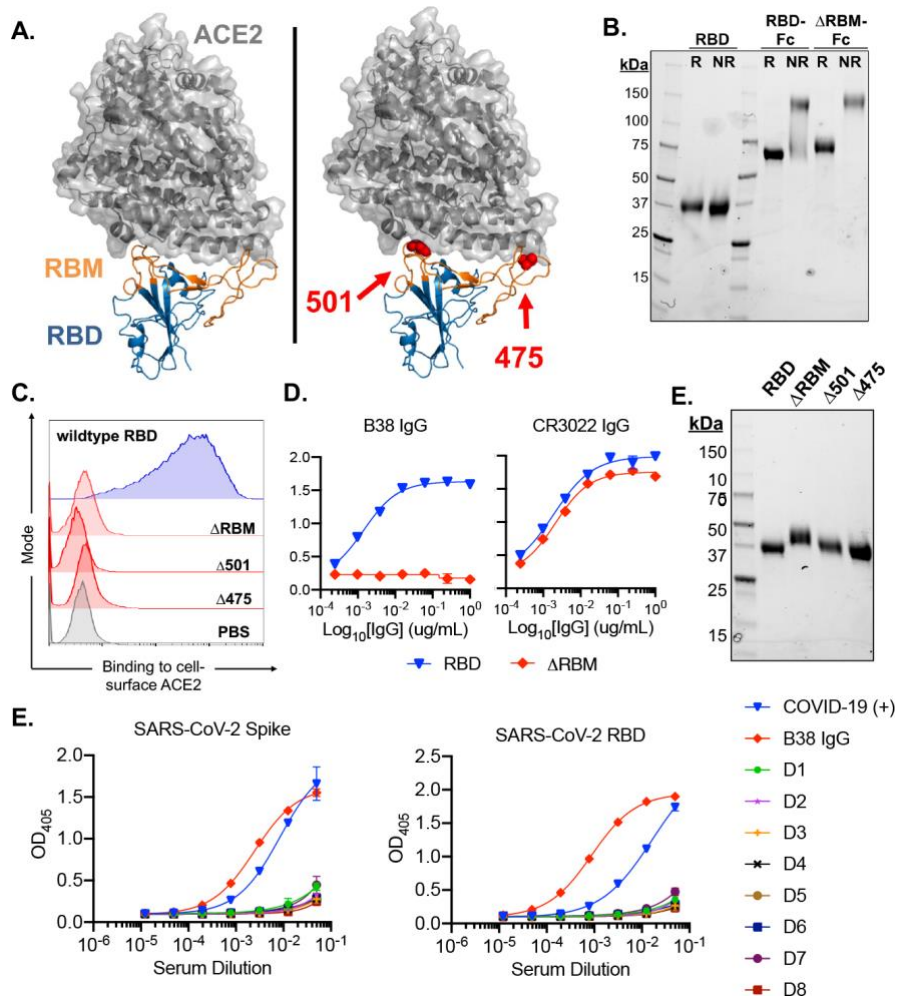
¹Ragon Institute of MGH, MIT and Harvard, Cambridge, MA, 02139, USA

²Department of Microbiology, Icahn School of Medicine at Mount Sinai, New York, NY 10029

³Department of Microbiology, Harvard Medical School, Boston, MA 02115, USA

*Correspondence to: Email: dlingwood@mgh.harvard.edu (D.L.); aschmidt@crystal.harvard.edu (A.G.S)

†These authors contributed equally to this work.

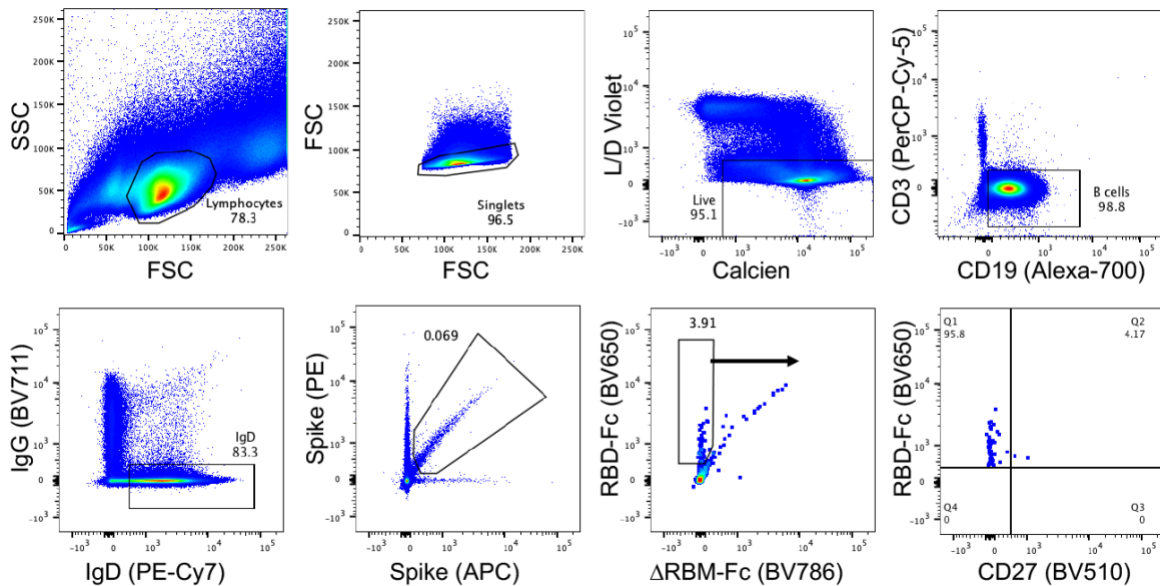


978
979

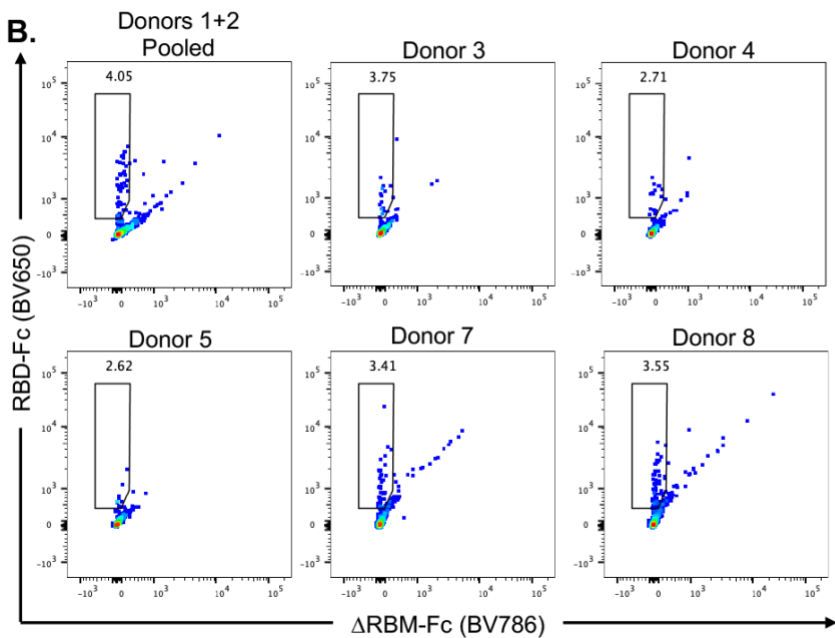
980 **fig. S1. Design and characterization of SARS-CoV-2 antigens and healthy donor sera**
 981 **binding.** (A) SARS-CoV-2 RBD in complex with viral receptor, ACE2 shown in blue and grey,
 982 respectively (PDB 6M0J). Wild-type RBD with, the receptor binding motif (RBM), shown in
 983 orange (left panel). Structural model of the Δ RBM probe designed to abrogate binding to ACE2
 984 (right panel). Putative N-linked glycosylation sites engineered onto the RBM are shown in red
 985 spheres at amino acid positions 501 and 475. (B) SDS-PAGE gel under reducing (R) and non-
 986 reducing (NR) conditions for monomeric RBD, RBD-Fc and Δ RBM-Fc. (C) Wildtype RBD,
 987 Δ RBM and single glycan variant binding to ACE2-expressing 293T cells by flow cytometry. Wild-
 988 type RBD binding shown in blue, glycan variant binding shown in red. Streptavidin-PE was used
 989 to detect the relative intensity of antigen binding to cell-surface ACE2. A PBS control (gray)
 990 indicates secondary-only staining. (D) Control antibody ELISA binding to RBD and Δ RBM
 991 antigens. RBM-specific antibody, B38 (left). Non-RBM-specific control antibody, CR3022
 992 (right). (E) Δ RBM and Δ 501 and Δ 475 variants analyzed by SDS-PAGE gel under reducing
 993 conditions; wildtype RBD is shown for comparison. (E) SARS-CoV-2 spike (left) and RBD (right)
 994 sera ELISA from human subjects 1-8. Sera from a COVID-19 convalescent patient and control
 995 antibody, B38, were included as positive controls.

A.

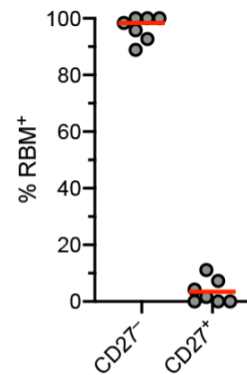
Sort Strategy Overview: Donor 6



B.

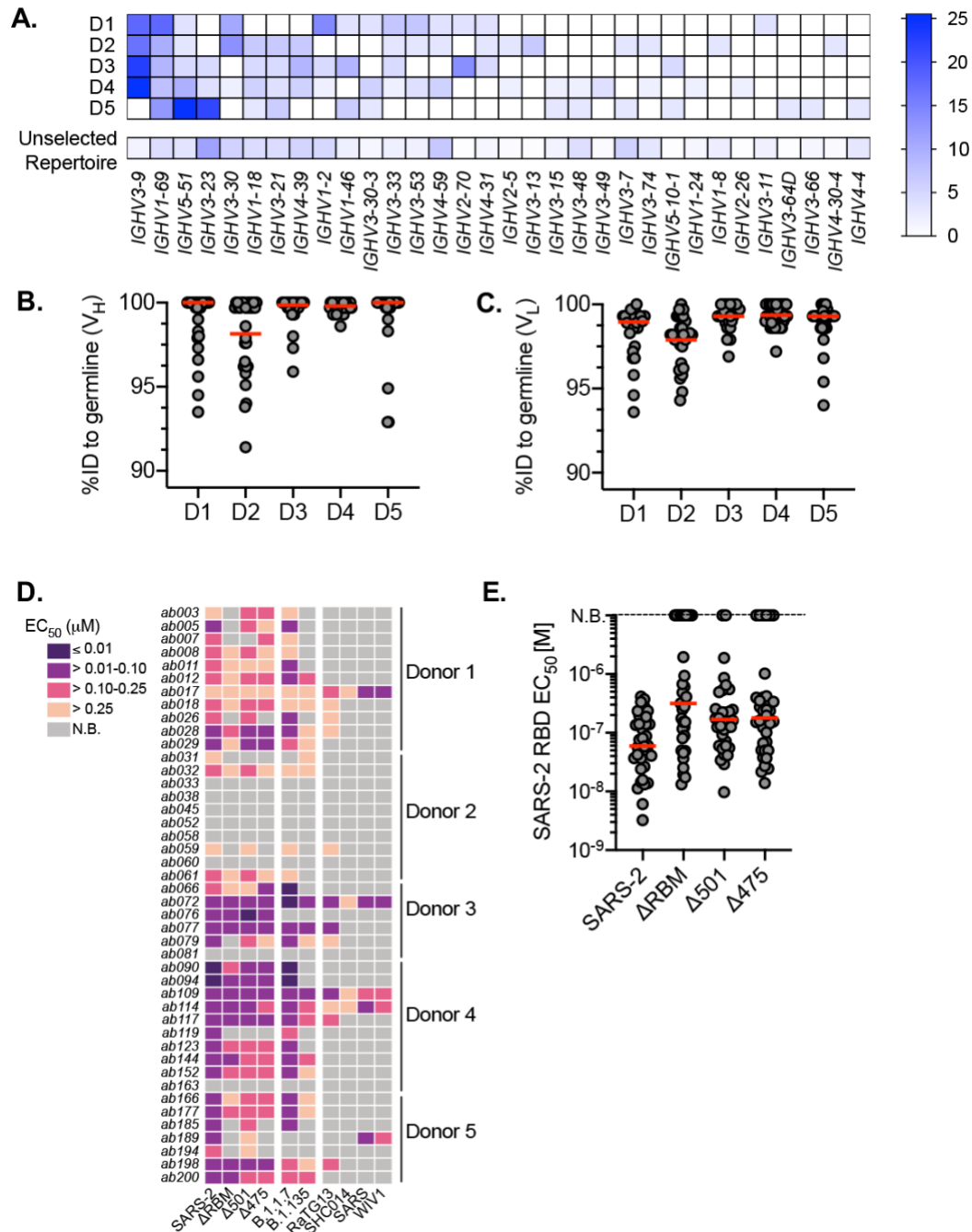


C.



996
997

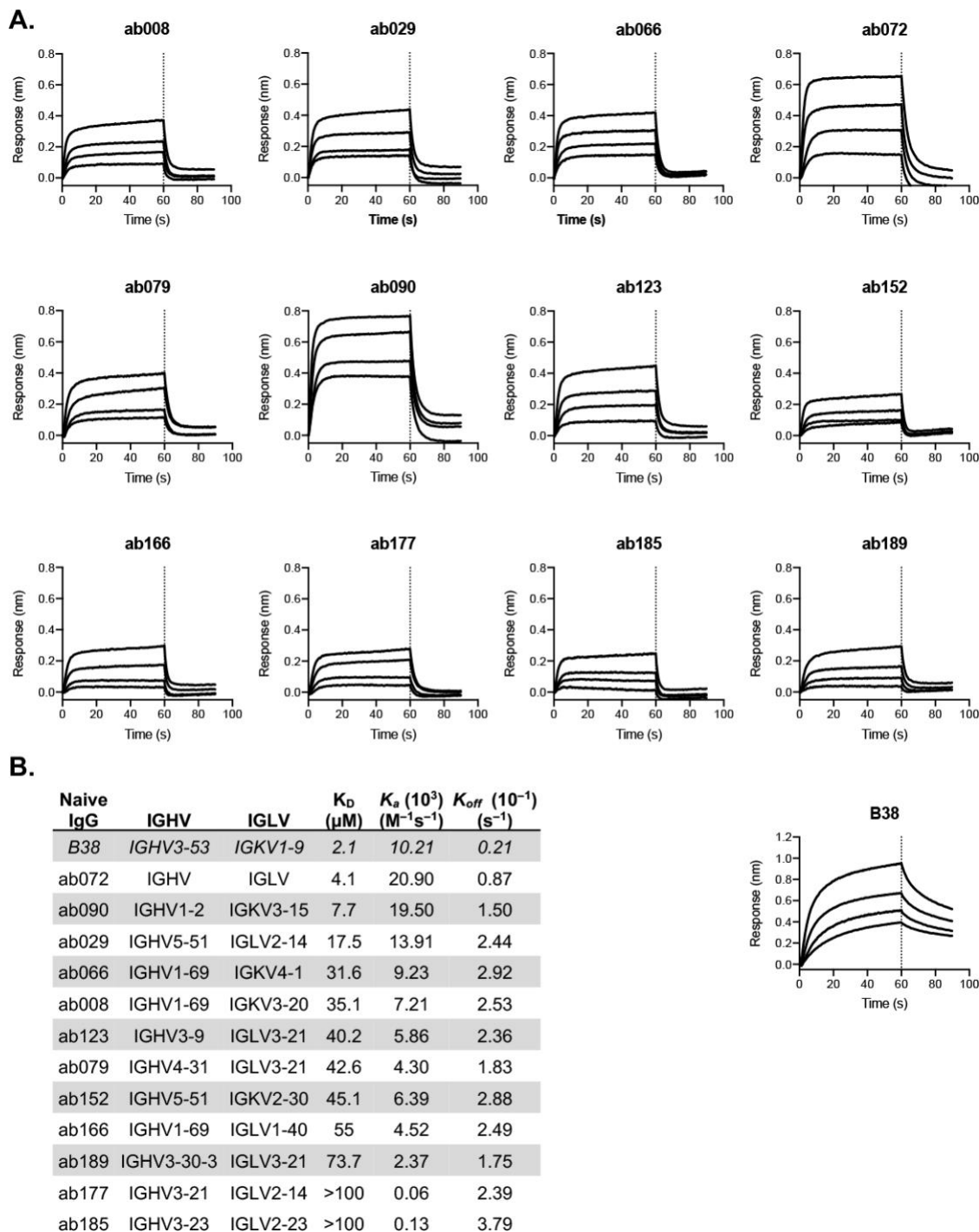
998 **fig. S2. PBMC flow cytometry analyses.** (A) Representative gating strategy used for FACS of
999 PBMCs pooled from donors 1 and 2. Gating was on naive B cells defined by single living
1000 lymphocytes that were CD19⁺CD3⁻IgD⁺IgG⁻. Sorted cells were RBM-specific as defined by spike-
1001 PE⁺/spike-APC⁺/RBD-Fc-BV650⁺/ΔRBM-Fc-BC650⁻. Sort gate is denoted by the blue arrow. The
1002 bottom right plot shows CD27 staining of sorted RBM-specific naive B cells. (B) Flow cytometry
1003 showing the sort gate and percentage of RBM-specific B cells for the remaining 6 healthy human
1004 donors. (C) RBM-specific B cell frequency among CD27⁺ and CD27⁻ cells. Each symbol
1005 represents a different donor ($n = 8$).



1006
1007

1008 **fig. S3. Repertoire comparison, germline identity, and IgG binding by individual donor.** (A)
1009 Heatmap showing V_H-gene usage of isolated antibodies derived from donors 1-5. Unselected
1010 repertoire gene usage derive from a high-throughput sequencing data set of circulating B cells
1011 across 10 human subjects (46). Heatmap scale represents percent of total paired sequence from
1012 each donor. Divergence from inferred germline gene sequences separated by individual donor for
1013 (B) V_H and (C) V_L. Red bars indicate the median percent values, and each dot represents an
1014 individual paired sequence. (D) Heatmap showing IgG binding to RBDs (n = 44) sorted by donor.
1015 (E) ELISA EC₅₀ values for IgGs with detectable SARS-CoV-2 RBD binding (n = 36) against RBM
1016 glycan probes. Red bars indicate the mean EC₅₀ values.

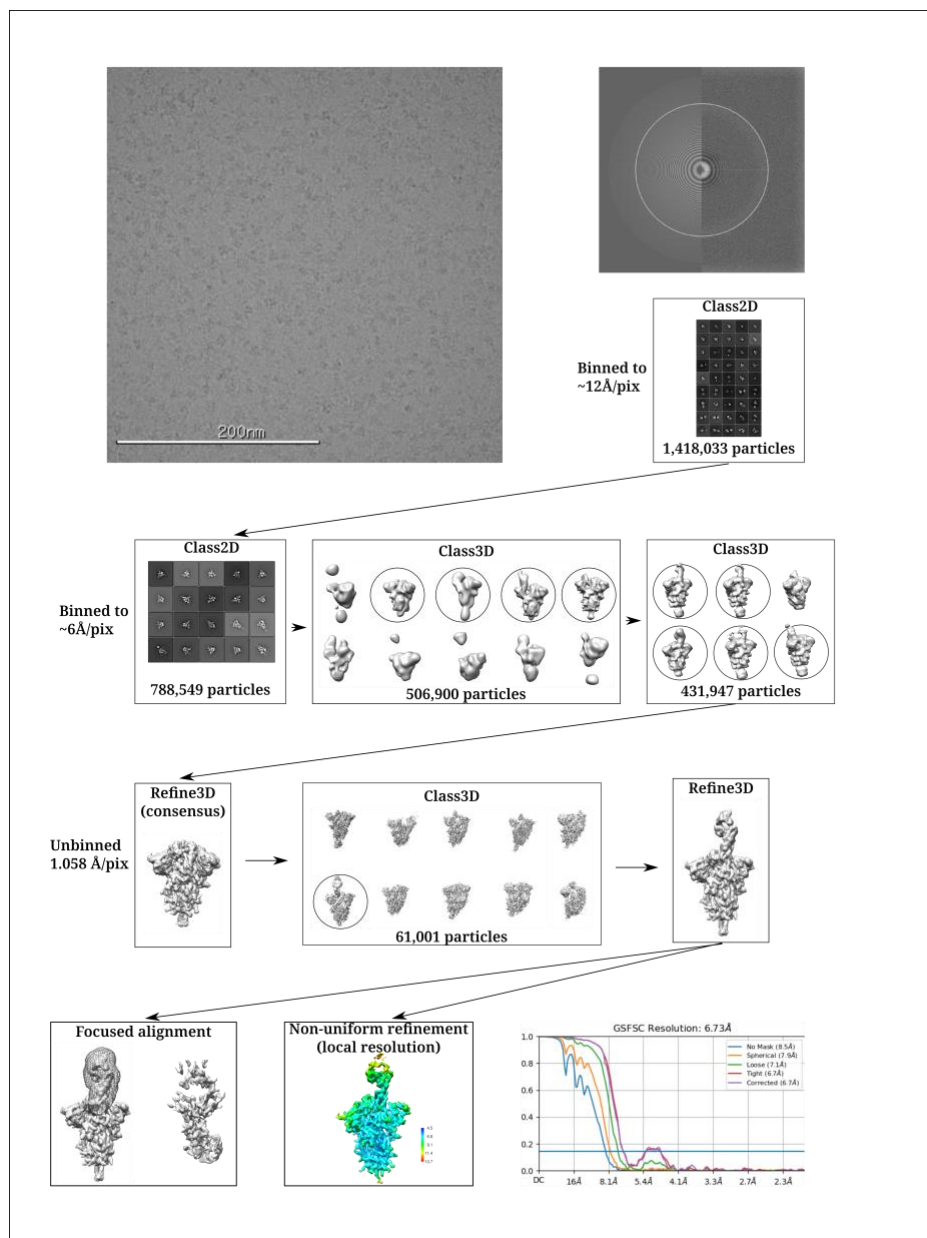
1017



1018
1019

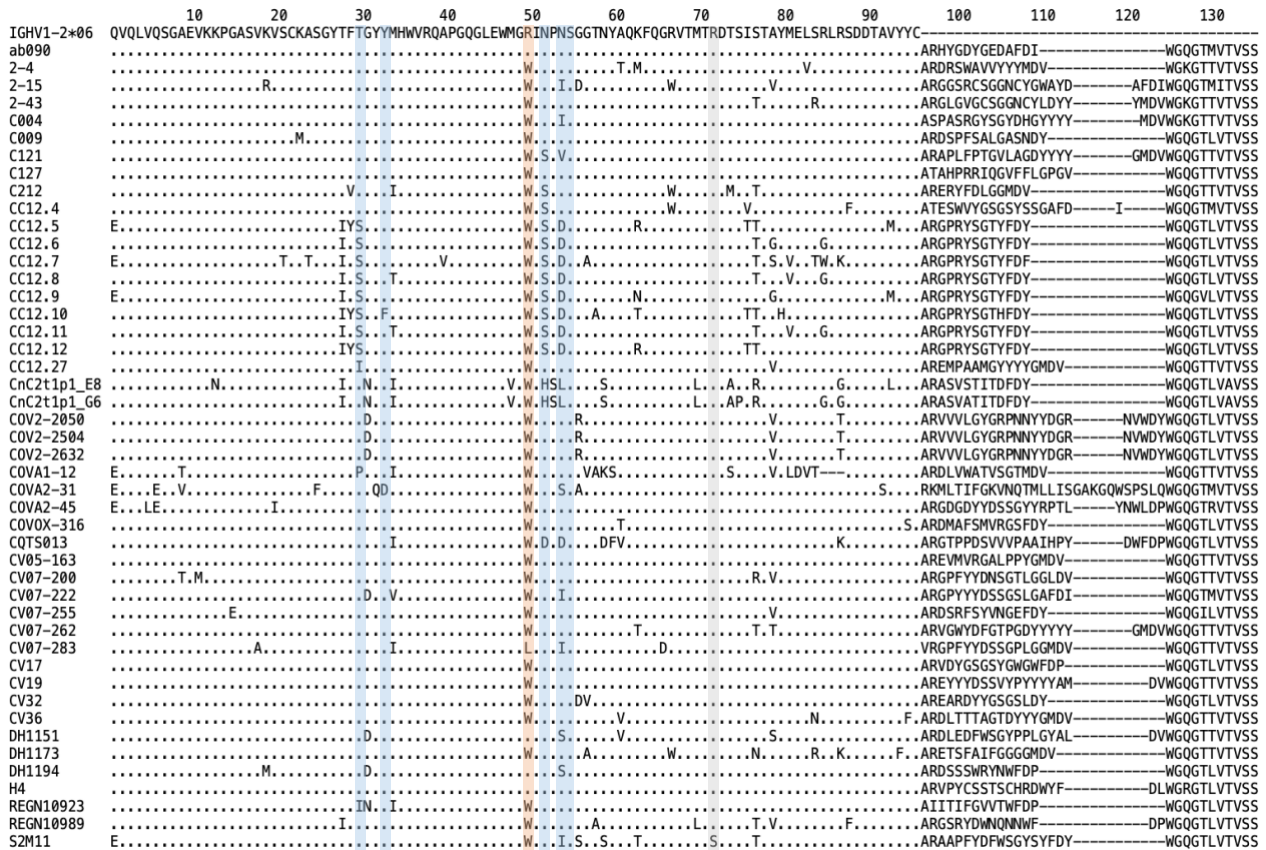
1020 **fig. S4. SARS-CoV-2 RBD-binding kinetics of isolated naive antibodies.** (A) Biolayer
1021 interferometry (BLI) binding kinetic analysis of titrated SARS-CoV-2 RBD to immobilized Fabs.
1022 Dotted line at 60 s denotes the start of the dissociation phase. (B) Kinetic and equilibrium constants
1023 for binding to RBD calculated from a 1:1 binding model using a global fit to all curves for each
1024 Fab using vendor supplied software. B38 Fab is used as a positive control.

1025
1026 **A.**



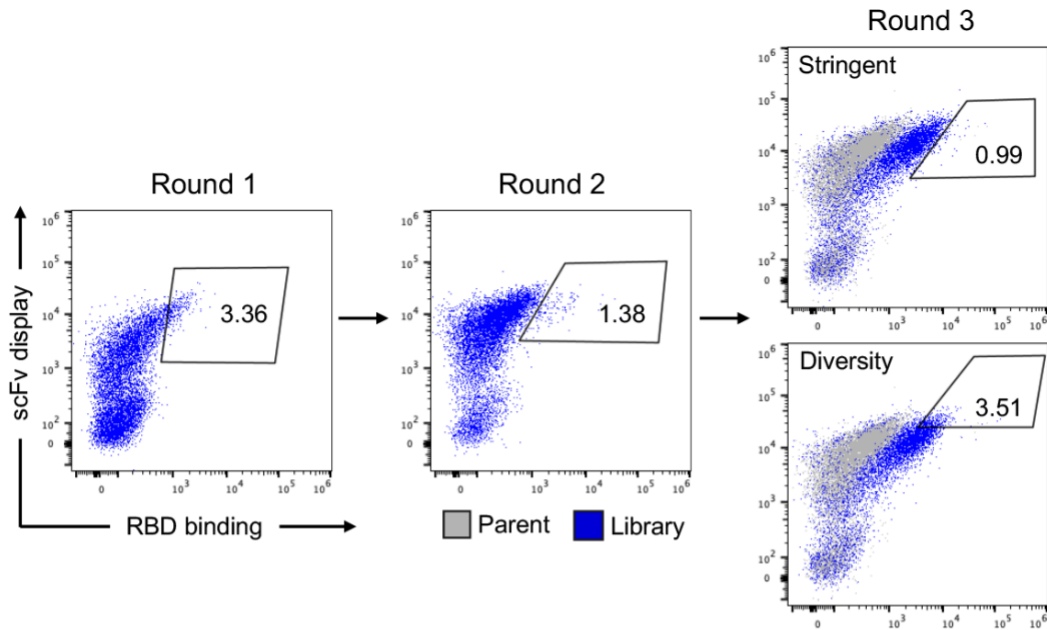
1027
1028

1029 **B.**

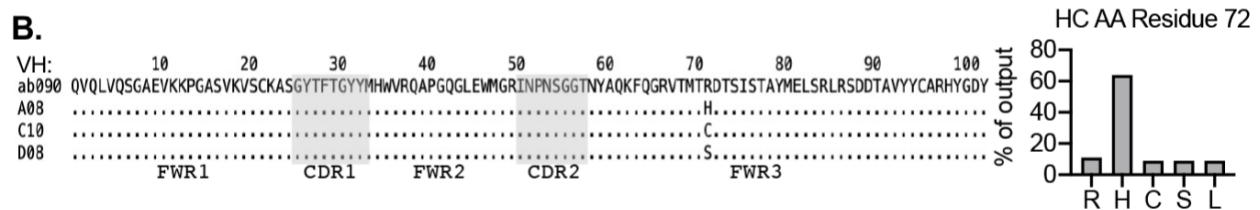


1030 **fig. S5. Structural characterization and analysis.** (A) Cryo-EM data processing scheme of
 1031 ab090 Fab bound with SARS-CoV-2 spike. See the Methods section for more details. (B) Heavy
 1032 chain amino acid sequence alignment of ab090 with IGHV1-2 derived antibodies from
 1033 convalescent COVID-19 patients. Sequences were obtained from CoV-AbDab (118) and aligned
 1034 to the IGHV1-2*06 reference. Residues forming the germline-encoded HCDR1 and HCDR2 motif
 1035 contacting the SARS-CoV-2 RBD are highlighted in blue. The single nucleotide polymorphism in
 1036 the *06 allele at position 50 is highlighted red. The site of the dominant mutation from *in vitro*
 1037 affinity maturation efforts with ab090 is highlighted in green.

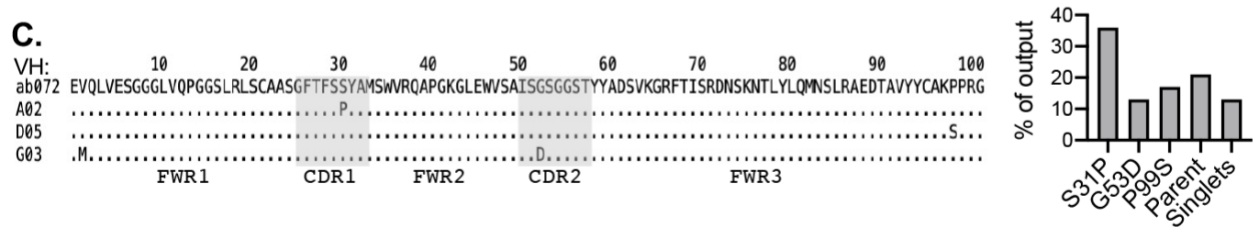
A.



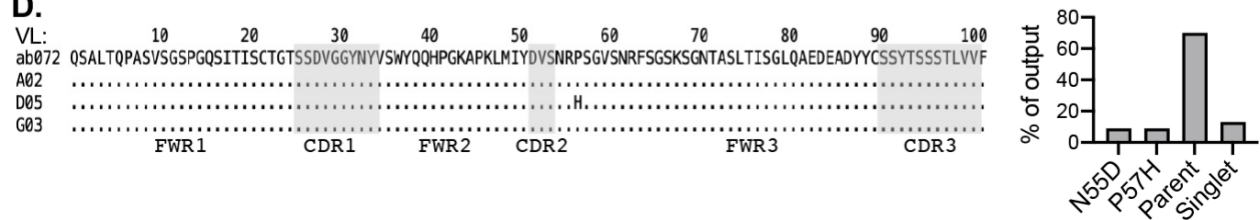
B.



C.



D.



1038
1039
1040
1041
1042
1043
1044
1045
1046
1047

fig. S6. Representative affinity maturation selection strategy and output sequence overview.

(A) Flow cytometric sorting of diversified single chain variable fragment (scFv) libraries of ab090. Gates represent the yeast population sorted for subsequent selections. After 2 rounds of enrichment for wildtype SARS-CoV-2 binding, a “stringent” and “diversity gate were sorted in round 3 indicating the yeast populations sorted for individual colony isolation and sequencing. Alignment of the V_H sequencing output clones for ab090 (B) and ab072 (C) with the output frequency of each mutation from a total of 48 single colonies. (D) Alignment of the V_L sequencing output clones ab072 with the output frequency of each mutation from a total of 48 single colonies. The V_L output for ab090 was exclusively parent.